Mid-Infrared High-Resolution Achromatic Air Microlens in Silicon

Haoran Mo(莫昊燃)[1†], Zitao Ji(纪子韬)[1†], Yidong Zheng(郑义栋)[1†], Huakang Yu(虞华康)[1], Wenyao Liang(梁文耀)[1], and Zhi-Yuan Li(李志远)[1,2*]

[1]*School of Physics and Optoelectronics, South China University of Technology, Guangzhou 510640, China*
[2]*State Key Laboratory of Luminescent Materials and Devices, South China University of Technology, Guangzhou 510640, China*

(Received 13 January 2025; accepted manuscript online 22 April 2025)

Infrared (IR) optics have garnered significant attention due to growing demands in advanced optical imaging, communication, detection, and sensing. Among various IR devices, microlenses and microlens arrays offer distinct advantages in integration capability, imaging precision, multifunctionality, and cost-effective manufacturing. We present a novel design of high-resolution achromatic microlens in the mid-IR region. Different from traditional high-refractive-index convex microlenses embedded within a low-index background medium, the current design is a low-index air concave microlens embedded within a high-index silicon medium. The designed air microlens exhibits capabilities in high-resolution imaging ($\sim\lambda/6$) and achromatic performance across the 3–5 μm mid-IR spectrum. The air microlens could be assembled in large-area microlens arrays or as part of multi-lens system. When combined with the HgCdTe detector system placed on the focal plane, the air microlens can find promising applications in high-resolution optical imaging and high-sensitivity photoelectric detection.

DOI: 10.1088/0256-307X/42/5/054201 CSTR: 32039.14.0256-307X.42.5.054201

1. Introduction. Infrared (IR) optics have been growing rapidly thanks to the demand for biomedical imaging,[1,2] high-capacity telecommunication,[3–5] high-precision metrology[6,7] and so on. All these systems rely on the integration, ultrafast response, and effective coupling of the compact, miniaturized, high-precision, and scalable optical elements. With the development of nanofabrication manufacturing, different materials, such as silicon, germanium, sapphire, and chalcogenide glasses, have been utilized for designing and fabricating IR devices, including waveguides, detectors, lasers, and imaging.[8,9] Among these, IR imaging systems have been widely used in military and civilian applications, such as focal plane detectors and hyperspectral detection.[9] Microlenses are one of the most essential elements in IR optical imaging systems. Recently, with the proposal of optical dielectric metasurfaces,[10,11] metalenses have gained a lot of attention.[12–14] IR metalenses have also been reported, which can cover a whole band from near IR to long-wave IR.[15–23] Among these, various approaches and schemes towards building broadband achromatic microlenses have been intensively and extensively discussed. One approach is a confocal achromatic scheme implemented through compensation of the propagation phase dispersion.[24] Another is via the integrated resonance method with smooth and linear dispersion.[15] Besides, with efforts in optimizing the structure parameters of each element in the metalens or utilizing phase-change materials like $Ge_2Sb_2Se_4Te_1$, achromatic microlens designs working for polarization-insensitive light have also been realized.[25] Very recently, a metalens focal plane array was fabricated for designing a sensitive photoelectric detector by utilizing the material GaSb in the mid-wave IR range.[26] There was also a report considering a new design of a bifocal metalens that works for different polarized incident light.[27]

Nonetheless, conventional refractive and diffractive lenses still have their own advantages compared with metalenses in imaging quality and manufacturing cost. The inherent limitation of metalenses makes it hard to reach a high numerical aperture (NA), and the manufacturing cost of metalenses is expensive. With the development of nano/microscale fabrication processing technologies, there have also been reports of different microscale refractive or diffractive lenses.[28–30] The concept of microlens array integration has gained a lot of attention, which is suitable for use in extremely miniaturized imaging systems and 3D light field cameras. Microlenses and microlens arrays could enhance the integration, precision, and multifunctionality of different systems, including communication, processing, sensing, and display systems. Up to now, different materials have been utilized for fabricating microlenses in the IR region, such as polymer microlens arrays in the near IR region,[31] ZnSe arrays[32] or directly etching of Si substrates.[33]

In this Letter, we demonstrate a novel design scheme of low index microlenses at the mid-IR window. Compared with the traditional scheme where microlenses were convex and composed of high index materials placed within a low index medium (usually air) for efficiently focusing light, our low index microlenses were concave and immersed in

†These authors contributed equally to this work.
*Corresponding author. Email: phzyli@scut.edu.cn
© 2025 Chinese Physical Society and IOP Publishing Ltd. All rights, including for text and data mining, AI training, and similar technologies, are reserved.

a high index background matrix. In Section 2, we show a design of air (the medium with the lowest refractive index) microlenses placed within a silicon substrate. Hereinafter, we unveil the achromatic properties of our air-based microlenses in Section 3, which are found to originate from the ultra-low dispersion of silicon substrate materials. Finally, in Section 4, we discuss different designs of our low index microlenses and then investigate the prototype design of our low refractive microlens system for opto-electronic detection. Our designed microlenses can be extended to construct large microlens arrays, which can be applied in IR imaging or as an element of multi-lens system.

2. Design of Air Microlens. Figure 1 contrasts the geometrical differences between the traditional and currently proposed scheme of microlens designs. Figure 1(a) illustrates the conventional approach with a high refractive index microlens, where the convex shape is necessary for focusing light. In contrast, figure 1(b) presents the innovative low refractive index microlens we propose in this work, which utilizes a concave shape in consistency with the air microlens configuration for realizing light focusing, according to Snell's law. The substrate material surrounding the concave low index microlens has a high refractive index. This unconventional design demonstrates superior performance in light focusing and imaging, aligning with the application and manufacturing processes of IR detectors, and is integrable onto the focal plane array of IR detectors. Our microlens is designed for working in the mid-wave IR window ranging from 3 to 5 μm. In this region, we choose silicon as the substrate material because it has a very high refractive index of ∼3.4–3.6 and very low dispersion. Then the air microlens is embedded within the silicon matrix to serve as a whole as a high-performance mid-wave IR focusing and imaging device.

In the mid-IR region, silicon has a high index, near-zero absorption, and low dispersion, which makes it extraordinarily useful in the design of high NA and achromatic microlenses. The dispersion formula of Si at room temperature can be fitted by Herzberger-type as below,[34,35]

$$n = A + BL + CL^2 + D\lambda^2 + E\lambda^4, \tag{1}$$

where $L = 1/(\lambda^2 - 0.028)$ with the wavelength λ in unit of micrometers. The coefficients are $A = 3.41906$, $B = 1.23172\times10^{-1}$, $C = 2.65456\times10^{-2}$, $D = -2.66511\times10^{-8}$, and $E = 5.45852\times10^{-14}$.

Figure 2 shows the calculated dispersion curve of Si in the mid-wave IR band. The index of refraction of Si changes from 3.433 to 3.424 when the wavelength varies from 3 to 5 μm. Therefore, only a 0.26% difference in refraction makes Si a suitable material for designing achromatic lenses in the mid-IR region. Ignoring possible absorption in Si, we show the FDTD simulations of the focusing of an incident electromagnetic (EM) plane wave. As illustrated in Fig. 3(a), since our structure is symmetrical in the *xoy*-plane, the simulations can be simplified into a 2D model

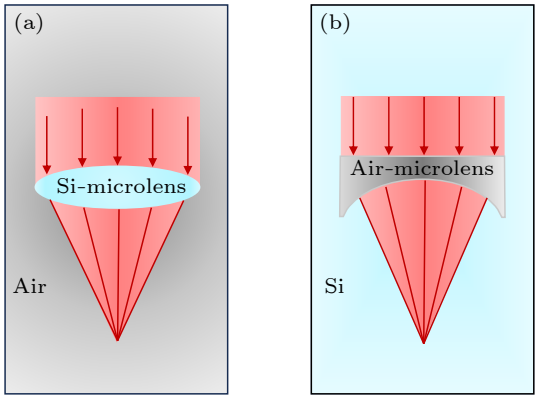

Fig. 1. Comparative analysis of the microlens designs. (a) The schematic of a traditional high refractive index microlens. (b) The schematic of the proposed low refractive index microlens, demonstrating the concave shape due to the air-based design.

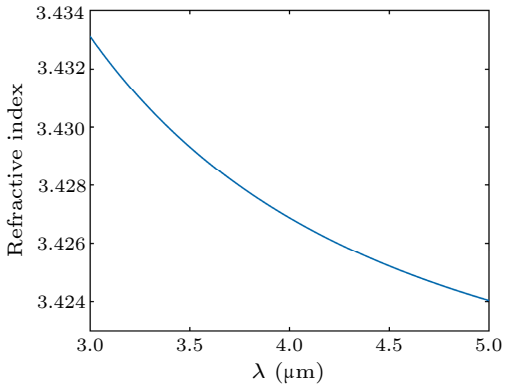

Fig. 2. The index of refraction of Si in the mid-IR window.

while the results are still reliable. Figures 3(b1) and 3(b2) show the simulation results of normally incident plane waves transmitting through our designed microlens when $\lambda = 4\,\mu$m. In this situation, the refractive index of Si is 3.427. The white frames in the shape of plano-concave lens are our designed air microlens.

The radius of the half concave surface is 50 μm and the minimum distance between the upper plane and down surface of the air microlens is 25 μm. The incident plane waves propagate along the z-axis, and the polarization state can be separately configured as transverse electric (TE) and transverse magnetic (TM) polarizations, where the field components of incident light for the TE polarization have E_y, H_x, and H_z, whereas those of the TM polarization correspond to H_y, E_x, and E_z. Both in TE and TM polarization cases, the simulations show that the incident plane waves converge after going through the air microlens. In order to characterize the focusing performance, figure 3(c) shows the optical intensity profile along the x-axis cross-section of focal spots in TE and TM cases. Apparently, the difference between TE and TM waves is very slight. The full width at half maximums (FWHMs) are 0.658 μm in the TE situation and 0.819 μm in the TM case. In Fig. 3(d), the optical intensity profile along the z-axis cross-section of focal spots shows the depth of fields (DOFs) with TE and TM incident waves.

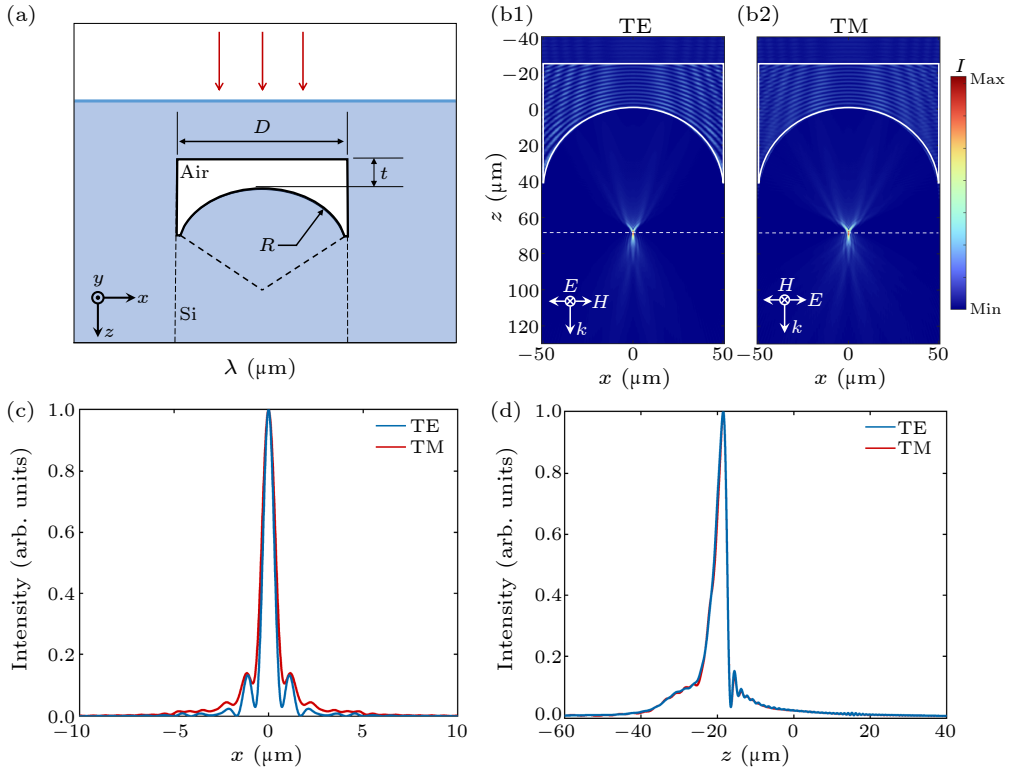

Fig. 3. (a) Illustration of the simulation structure. D, t, and R respectively denote the diameter, thickness, and the radius of the concave surface of the air microlens. (b1) and (b2) The simulation results of optical focusing for the air microlens in TE and TM cases. The EM plane waves are normally incident from the top. (c) and (d) The electric field distributions along the x-axis and z-axis cross-section of the focal point, respectively.

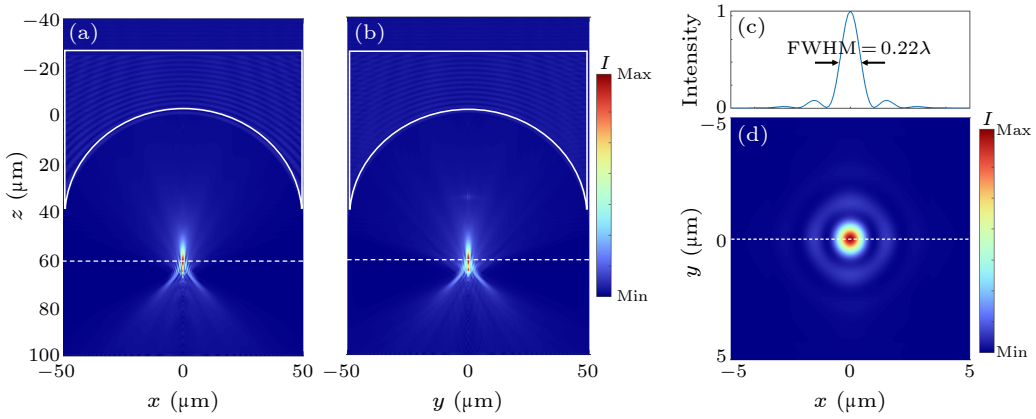

Fig. 4. The 3D simulation results of optical focusing for the air microlens. The EM plane waves are normally incident from the top with a linear polarization aligned along the y-axis. (a) and (b) The intensity distribution in the xoz-plane and yoz-plane cross-sections, respectively. (c) The one-dimensional intensity profile along the white dashed line in (d), which illustrates the intensity distribution of the xoy-plane cross-section at the focal point.

In the TE case, the FWHM of DOF is 3.515 μm, and 3.316 μm in the TM case. A much larger DOF than the FWHM in the x-axis shows the spherical aberration in our system. Since the system cannot be regarded as a thin lens, we define the back focal distance as the focal length, which is the distance from the last optical surface to the focal point. Therefore, the focal lengths are 68.345 μm in the TE case and 68.284 μm in the TM situation. Due to the high refractive index of Si, the design of a high NA lens is easily accessible. To show the NA limit of our system, a whole hemisphere is considered as the down surface of the air microlens. As is well known, the NA can be defined as $\mathrm{NA} = n \sin\theta$, where n is the index of refraction of the medium within which the lens is working, and θ is the half angle of the maximum cone of light that can enter or exit the lens. Therefore, according to the simulations, the NA is up to 3.214 in both the TE and TM cases.

To substantiate the accuracy of our 2D modeling, we conducted a 3D simulation of the simulation model corresponding to Fig. 2(b). The simulation was executed with linearly polarized plane waves incident along the z-axis and possessing a wavelength of 4 μm. As shown in Figs. 4(a) and 4(b), the 3D simulation yields a focal length of 60.6 μm and a depth of focus measuring 7.4473 μm. Additionally,

the FWHM at the focal point is measured at 0.8867 μm in the *xoz*-plane cross-section and 0.9753 μm in the *yoz*-plane cross-sections. The dimensional discrepancy between 3D and 2D models results in variations in the lens's focusing efficacy. The 2D model serves as a simplified abstraction of the 3D construction, leading to discrepancies in the results along the optical axis, such as the focal length and DOF. However, due to the rotational symmetry of the air lens, the difference is small in the transverse plane at the focal point, as shown in Figs. 4(c) and 4(b), rendering the 2D simulation outcomes sufficiently reliable for reference.

3. Small Chromatic Aberration of Air Microlens within Silicon Substrate. As mentioned before, due to the weak negligible material dispersion of Si in this wavelength region, the chromatic aberration in our designed microlens is already relatively slow, even without the need for careful and special design for handling the achromatic issue. In Fig. 5, we show the simulation results of optical focusing from 3 to 5 μm at the mid-IR band. The focal points remain small in both cases of TE and TM wave incidence. The FWHMs of the focal points are only one quarter of the incident wavelengths. When the wavelength becomes larger, the refractive index of Si slightly decreases, resulting in a larger focal spot size.

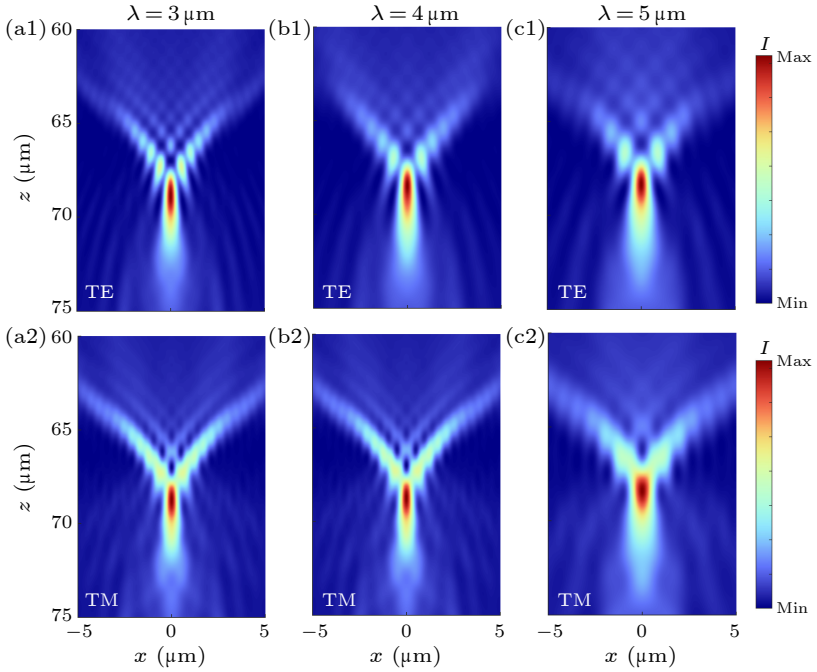

Fig. 5. The simulation focusing results of air microlens in TE and TM cases. (a) $\lambda = 3\,\mu m$. (b) $\lambda = 4\,\mu m$. (c) $\lambda = 5\,\mu m$.

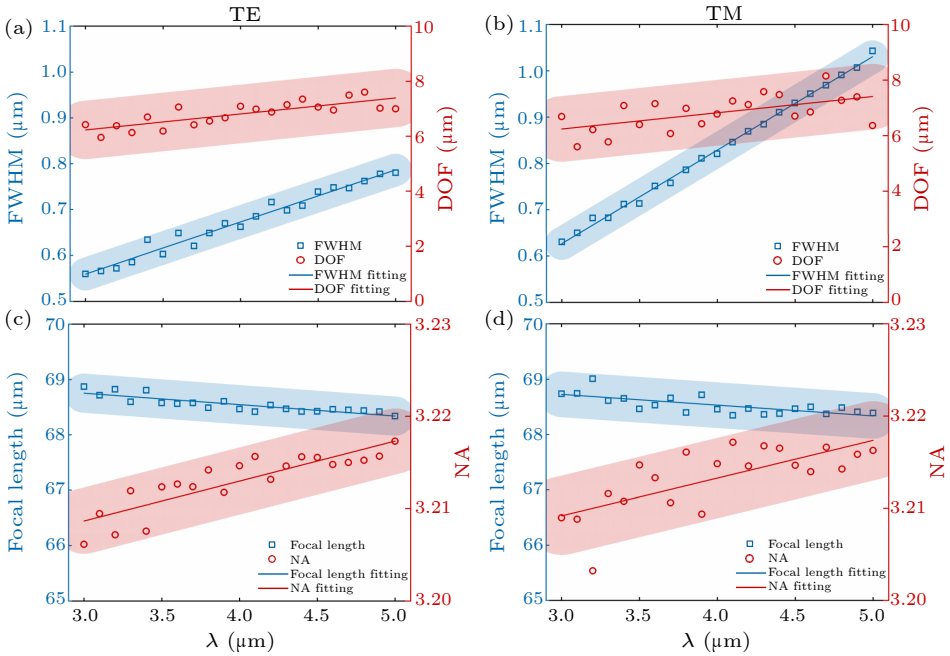

Fig. 6. (a) and (b) The FWHM and DOF changes from 3 to 5 μm in TE and TM cases, respectively. (c) and (d) The focal length and NA changes from 3 to 5 μm in TE and TM cases, respectively.

Figures 6(a) and 6(b) show the FWHM of the x-axis cross section of the focal spot. In the TE transmission case, the FWHM starts from 0.560 μm and increases to 0.781 μm when the wavelength changes from 3 to 5 μm, while the FWHM in the TM case is larger and starts from 0.630 to 1.041 μm. Therefore, the size of the focal spot undergoes less than 0.411 μm change in the mid-IR window, which is all connected with the barely changed refractive index of silicon. The difference between TE and TM incident plane waves may be due to the different EM components in TE and TM polarizations since TE polarization has E_y, H_x, and H_z, while TM polarization is related with H_y, E_x, and E_z, which will lead to discrepancies in the distribution of electric fields.

The focal length, DOF, and NA changes with respect to wavelength are also presented in Fig. 6. With the wavelength becoming larger, the focal length gradually becomes shorter, which results in the growth of NA. The DOFs remain high, showing a large spherical aberration in our systems. Regardless of this, all these changes are slight due to the superior low difference in the refractive index (i.e., low dispersion) within the 3–5 μm window. Therefore, our air microlens is suitable for designing achromatic lenses in the IR region. The oscillatory behavior evident in Fig. 6 is attributed to the unique design of the microlens system, where the refractive index of the lens material is lower than that of the substrate medium. This configuration results in the formation of a resonant cavity, leading to a quick interference effect within the front and back surfaces of the microlens. This interference effect significantly influences the apparent focal length's dependence on wavelength. As the wavelength varies, the cavity's resonant modes change, causing the focal length to exhibit periodic variations. An efficient way to remove such oscillatory behavior is to introduce anti-reflection coatings on the two surfaces of the microlens.

In the aforementioned design of the air microlens, we fix the radius of the half concave microlens as 50 μm and the incident wavelength of light is set as 4 μm. Apparently, the curvature of the lens is related to the focusing capability. In Fig. 7, we calculated the simulation results with different radii of the half concave surface. When the radius is changed from 20 to 70 μm, the focal length increases from 27.387 to 96.324 μm, showing that the ability to focus is related to the size of the air microlens. In contrast to the large alteration of focal lengths, the FWHM of the focal points only changes from 1.059 to 1.282 μm, which is still much smaller than the working wavelength. At the same time, the NA of the air microlens is maintained near 3.2 when the radius increases from 20 to 70 μm, which is unaffected by changes in the focal lengths. The DOF will shrink if the radius becomes smaller. It can be seen that the focusing ability will grow when the radius of air microlens is small. However, the total size of the incident light passing through the microlens will become less, leading to lower transmission total power, and this should be fully considered in the microlens design. Since the FWHM of the focal spot changes very little during our simulations. Therefore, to a large extent, we can flexibly design different sizes of air microlenses while at the same time maintaining a high resolution of focusing and imaging.

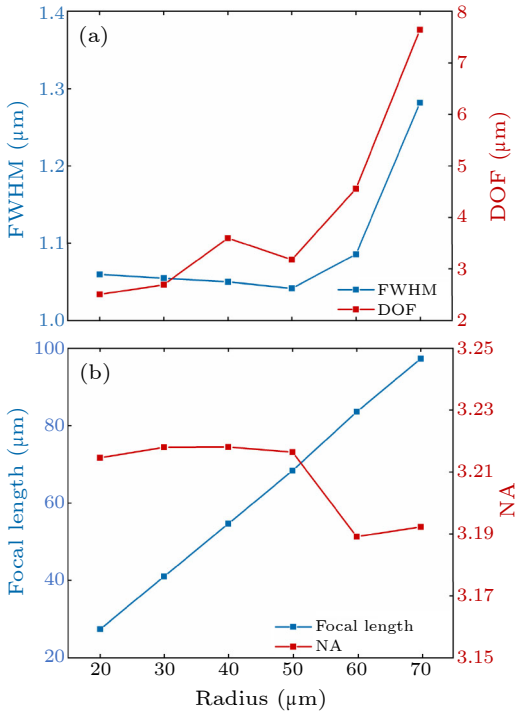

Fig. 7. The simulation results of the focal points with different radii of the air-based microlenses. The working wavelength is set as 4 μm, and the incident light is TM polarization in all simulations, and the substrate is Si. (a) The FWHM (blue line) of the focal points and the focal lengths (red line) with different radii. (b) The DOF (blue line) and the NA (red line) of the focal points with different radii.

4. Design of High-Sensitivity Photodetector. The above study has clearly shown that the air microlens embedded within a silicon substrate can achieve a very high NA that is not possible for ordinary structures of high-index microlenses embedded in low-index media like air, and generate a focal spot nearly 4 times smaller than the incident light wavelength (in air). This extraordinarily strong focusing power can be very useful in building high-sensitivity mid-IR photodetectors when this achromatic air/silicon microlens is incorporated with some appropriate mid-IR semiconductor materials in an appropriate geometric configuration. Here we find that HgCdTe is such a semiconductor material.

The ternary Ⅱ–Ⅵ compounds mercury-cadmium telluride or $Hg_{1-x}Cd_xTe$ (HgCdTe) are essential commercial materials for IR detectors. As a pseudo-binary alloy semiconductor, HgCdTe has a direct energy gap, high absorption coefficient, high mobility of electrons, and fast response time.[8,36] In application, the HgCdTe detector is used to fit our achromatic air/silicon microlens. As the Cd composition changes, the HgCdTe detectors for IR sensing and imaging can cover a wide spectral range from 1 to 30 μm, including from the short-wave IR to very-long-wave IR bands. The dispersion of its refractive index is

related to composition x and temperature T, which can be described as[37]

$$n(\lambda, T)^2 = A + B/[1 - (C/\lambda)^2] + D\lambda^2, \quad (2)$$

where the fitting parameters A, B, C, and D are given as follows:

$$\begin{aligned} A &= 13.173 - 9.852x + 2.909x^2 + 10^{-3}(300 - T), \\ B &= 0.83 - 0.246x - 0.0961x^2 + 8 \times 10^{-4}(300 - T), \\ C &= 6.706 - 14.437x + 8.531x^2 + 7 \times 10^{-4}(300 - T), \\ D &= 1.953 \times 10^{-4} - 0.00128x + 1.853 \times 10^{-4}x^2. \end{aligned} \quad (3)$$

As mentioned earlier, the difference in the refractive index of Si in 3–5 μm is only 0.26%, and this unique feature makes Si a suitable material for designing achromatic lenses in the IR region. At the same time, in order to match the refraction of Si, the composition of Cd in HgCdTe is set to be $x = 0.36$, and the refractive index changes from 3.609 at 3 μm to 3.167 at 5 μm. As little as possible difference between the refraction indexes of Si and HgCdTe can maintain high NA and a small focus point for imaging in the focal plane.

Figure 8(a) represents the configuration where the air microlens is embedded within a silicon medium, which is compatible with the HgCdTe material used in IR detectors, facilitating integration onto the focal plane array of such detectors. Figure 8(b1) shows the results of normal incident plane waves transmitting into our designed microlens when $\lambda = 4$ μm. In this situation, the refraction of Si is 3.427 and $Hg_{0.64}Cd_{0.36}Te$ is 3.357. The white frames in the shape of a plano-concave lens are our designed air-based microlens, and the white dashed lines separate the substrate and detector regions, with Si above and HgCdTe below.

The key design in our air-based microlens is that a highly matched optical detector material HgCdTe fits snugly to the Si substrate. Therefore, a very small focal point can be maintained during the transmission of light due to the impedance matching of different materials. Figure 8(b2) shows the case when the incident light emits from the Si substrate into the air. In this situation, most of the light will undergo total reflection, forming a spot inside the Si substrate. A focal spot can still be identified in the air region, formed by the output of remaining light. However, compared with the focal spot in the HgCdTe medium, the power of the emission into the air is less, and the focal point becomes wider. As shown in Fig. 8(c), the FWHM of the focal spot in air is about 1.548 μm, whereas in the HgCdTe case, the focal spot is only 0.690 μm. Therefore, the index match between Si and HgCdTe eliminates total reflection. With no air space between the Si substrate air-based microlenses and HgCdTe detection region, high-resolution imaging with an ultra-sub wavelength focal spot can be obtained.

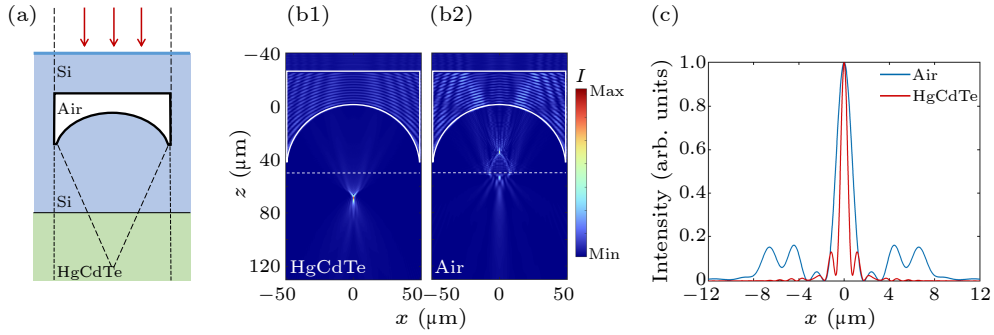

Fig. 8. (a) Schematic illustration of the integration of a silicon substrate with the optical detector material HgCdTe for an air microlens. (b) The simulation result of TE incident light at 4 μm. The white line shows the region of the air microlens with a radius of 50 μm. The white dashed line shows the interface between Si substrate and HgCdTe (b1) or air (b2). (c) The FWHM of focal points along the focal plane. The red line shows the case of focal spot inside HgCdTe medium. The blue line represents the focal spot in the air, which corresponds with the left simulation result.

5. Conclusion. In conclusion, we have proposed a novel design of low-refractive-index microlens working in the mid-IR region. Compared with traditional high-index convex microlenses, our design features a plano-concave microlens surrounded by a high-index substrate. In the 3–5μm window, Si has ultra-low dispersion with a high refractive index; therefore, our air-based microlenses with Si substrate have the characteristics of achromatic and high-resolution imaging. The focal spots are less than one-quarter the width of the working wavelength. Furthermore, we could precisely design different types of air-based microlenses, such as double concave shape or convexo-concave shape, which show potential in expanding the function of air-based microlenses for different demands. Since Si could be easily compatible with CMOS processes, the assembly of air-based microlenses with HgCdTe systems in the focal plane could be applied in the high-performance IR detectors market, which has shown a fervent desire for lower cost, larger array format size, high operating temperature, and multi-band detection. Considering these factors, our air-based microlenses are suitable for designing large-area microlens arrays or as one element of multi-lens systems. Furthermore, the operational spectrum of air-based microlenses can be extended beyond the mid-IR regime by leveraging the broadband IR transparency of monocrystalline silicon with varying purity levels and the wide spectral coverage of HgCdTe detectors spanning from near- to

far-IR bands.

Acknowledgements. This work was supported by the Science and Technology Project of Guangdong Province, China (Grant No. 2020B010190001), the National Natural Science Foundation of China (Grant No. 12434016), and the National Key Research and Development Program of China (Grant No. 2018YFA0306200).

References

[1] Beć K B, Grabska J, and Huck C W 2020 *Molecules* **25** 2948
[2] Beć K B, Grabska J, and Huck C W 2020 *Anal. Chim. Acta* **1133** 150
[3] Shen L, Ren H, Huang M, Wu D, and Peacock A C 2020 *Opt. Commun.* **463** 125437
[4] Flannigan L, Yoell L, and Xu C Q 2022 *J. Opt.* **24** 043002
[5] Fang Y, Ge Y, Wang C, and Zhang H 2019 *Laser Photon. Rev.* **14** 1900098
[6] Kim D W, Su T, Su P, Oh C J, Graves L, and Burge J 2015 *SPIE News*
[7] Wang H L, You E M, Panneerselvam R, Ding S Y, and Tian Z Q 2021 *Light: Sci. Appl.* **10** 161
[8] Lei W, Antoszewski J, and Faraone L 2015 *Appl. Phys. Rev.* **2** 041303
[9] Hou F, Zhang Y, Zhou Y, Zhang M, Lv B, and Wu J 2022 *Sustainability* **14** 11161
[10] Chen H T, Taylor A J, and Yu N 2016 *Rep. Prog. Phys.* **79** 076401
[11] Lee Y, Kim S J, Park H, and Lee B 2017 *Sensors* **17** 1726
[12] Aieta F, Genevet P, Kats M A, Yu N, Blanchard R, Gaburro Z, and Capasso F 2012 *Nano Lett.* **12** 4932
[13] Zhao Z, Pu M, Gao H, Jin J, Li X, Ma X, Wang Y, Gao P, and Luo X 2015 *Sci. Rep.* **5** 15781
[14] Yang W, Zhou J, Tsai D P, and Xiao S 2024 *Photon. Insights* **3** R04
[15] Wang S, Wu P C, Su V C, Lai Y C, Hung Chu C, Chen J W, Lu S H, Chen J, Xu B, Kuan C H, Li T, Zhu S, and Tsai D P 2017 *Nat. Commun.* **8** 187
[16] Yoon G, Kim K, Kim S U, Han S, Lee H, and Rho J 2021 *ACS Nano* **15** 698
[17] Fan Q, Liu M, Yang C, Yu L, Yan F, and Xu T 2018 *Appl. Phys. Lett.* **113** 201104
[18] Huang L, Coppens Z, Hallman K, Han Z, Böhringer K F, Akozbek N, Raman A, and Majumdar A 2021 *Opt. Mater. Express* **11** 2907
[19] Ou K, Yu F, Li G, Wang W, Chen J, Miroshnichenko A E, Huang L, Li T, Li Z, Chen X, and Lu W 2021 *Laser Photon. Rev.* **15** 2100020
[20] Xiao X, Zhao Y, Ye X, Chen C, Lu X, Rong Y, Deng J, Li G, Zhu S, and Li T 2022 *Light-Sci. Appl.* **11** 323
[21] Wang Z, Liu W, Zhu Y, and Zhou S 2024 *Appl. Opt.* **63** 2241
[22] Xu F, Chen W, Li M, Liu P, and Chen Y 2023 *Opt. Express* **31** 36439
[23] Yuan Y, Yan Z, Zhang P, Chang Z, Peng F, Chen R, Yang Z, Chen S, Zhao Q, and Huang X 2022 *Photonic Sens.* **13** 230126
[24] Li Y, Li X, Pu M, Zhao Z, Ma X, Wang Y, and Luo X 2016 *Sci. Rep.* **6** 19885
[25] Bai W, Yang P, Huang J, Chen D, Zhang J, Zhang Z, Yang J, and Xu B 2019 *Sci. Rep.* **9** 5368
[26] Zhang S, Soibel A, Keo S A, Wilson D, Rafol S B, Ting D Z, She A, Gunapala S D, and Capasso F 2018 *Appl. Phys. Lett.* **113** 111104
[27] He H, Yang H, Xie Z, and Yuan X 2022 *Nanoscale* **14** 12476
[28] Jiang H and Zeng X 2013 *Microlenses: Properties, Fabrication and Liquid Lenses* (Taylor & Francis)
[29] Yuan W, Li L H, Lee W B, and Chan C Y 2018 *Chin. J. Mech. Eng.* **3** 16
[30] Stevens R and Miyashita T 2013 *Imaging Sci. J.* **58** 202
[31] Liu F, Yang Q, Chen F, Zhang F, Bian H, and Hou X 2019 *Opt. Lett.* **44** 1600
[32] Zhang F, Yang Q, Bian H, Liu F, Li M, Hou X, and Chen F 2020 *IEEE Photonics Technol. Lett.* **32** 1327
[33] Sun Q, Tang J, Shen L, Lan J, Shen Z, Xiao J, Chen X, Zhang J, Wu Y, Xu J, and Wang X 2022 *Micromachines* **13** 899
[34] Herzberger M and Salzberg C D 1962 *J. Opt. Soc. Am.* **52** 420
[35] Palik E D 1991 *Handbook of optical constants of solids II* (Academic Press) **2** p. 599
[36] Rogalski A 2005 *Rep. Prog. Phys.* **68** 2267
[37] Liu K, Chu J H, and Tang D Y 1994 *J. Appl. Phys.* **75** 4176